Supporting Information for Complete transport of intensity equation for phase retrieval of optical vortex beams

Jialin Zhang[a,c,d,g,1], Runnan Zhang[a,c,d,1], Long Tian[b,1], Zhenwei Xie[e], Jiasong Sun[a,c,d], Shijun Zhu[f], Xiaocong Yuan[e,*], Qian Chen[a,d,*], Chao Zuo[a,c,d,*]

[a]*Smart Computational Imaging Laboratory (SCILab) School of Electronic and Optical Engineering Nanjing University of Science and Technology Nanjing Jiangsu 210094 China*
[b]*School of Mathematics and Statistics Nanjing University of Science and Technology Nanjing Jiangsu 210094 China*
[c]*Smart Computational Imaging Research Institute (SCIRI) of Nanjing University of Science and Technology Nanjing Jiangsu 210019 China*
[d]*Jiangsu Key Laboratory of Spectral Imaging & Intelligent Sense Nanjing University of Science and Technology Nanjing Jiangsu 210094 China*
[e]*Nanophotonics Research Center Shenzhen University 518060 Shenzhen China*
[f]*School of Science Nanjing University of Science and Technology Nanjing Jiangsu 210094 China*
[g]*Research Center for Intelligent Information Technology Nantong University Nantong Jiangsu 226019 China*

Abstract

This document provides supplementary information for "Transport of intensity equation for optical vortex beams". This supplementary information includes the derivation of the new formula, the comparison with the previous one, the validity of the new formula, and the supplement of the simulation and experiment of the proposed method.

Keywords: Transport of intensity equation (TIE), Orbital angular momentum (OAM)

*Corresponding authors.
Email addresses: xcyuan@szu.edu.cn (Xiaocong Yuan), chenqian@njust.edu.cn (Qian Chen), zuochao@njust.edu.cn (Chao Zuo)
[1]These authors contributed equally to this work.

Contents

Appendix A. The derivation of the complete transport of intensity equation (TIE) for optical vortex beams

The convention form of TIE can be written as the following equation of continuity [1]

$$-k\frac{\partial I\left(\mathbf{r},z\right)}{\partial z}=\nabla\cdot\left[I\left(\mathbf{r},z\right)\nabla\varphi\left(\mathbf{r},z\right)\right]. \tag{S.1}$$

where k is the wave number, $\mathbf{r}=(x,y)^T$ is the 2D position vector, $\nabla=(\partial_x,\partial_y)^T$ is the 2D gradient. To simplify the formula, we will omit $(\mathbf{r},z)$ in the following content. The phase (including vortices) change of the circuit encompassing the nodal point in $\mathbb{R}^2$ can be quantized as [2]

$$\oint_L \nabla\varphi dl=2m\pi\neq 0, \tag{S.2}$$

where the integer m is the topological charge of the singularity. For $m\neq 0$, $\nabla\varphi$ is not a gradient field. So one can separate it into two parts by using the Helmholtz decomposition. That is

$$\nabla\varphi=\nabla\phi_s+\nabla\times\beta, \tag{S.3}$$

where ϕ_s represents the gradient phase (scalar phase). Here the term $\nabla\times\beta=(-\beta_y,\beta_x)$ is divergence-free. Then Eq. S.3 is put into Eq. S.1 and we can obtain

$$\begin{aligned}-k\frac{\partial I}{\partial z}&=\nabla\cdot\left(I\nabla\phi_s+I\nabla\times\beta\right)\\&=\nabla\cdot\left(I\nabla\phi_s\right)+\nabla I\cdot\nabla\times\beta.\end{aligned} \tag{S.4}$$

From the Green's formula, for any closed contour L around the phase singular point we have

$$\begin{aligned}2m\pi=\oint_L\nabla\varphi dl&=\oint_L\nabla\phi_s dl+\oint_L\nabla\times\beta dl\\&=0+\oint_L-\beta_y dx+\beta_x dy=-\iint_D\Delta\beta dxdy,\end{aligned} \tag{S.5}$$

where $D\subseteq\mathbb{R}^2$ with $\partial D=L$. This means that $-\Delta\beta=2m\pi\cdot\delta_0$, where δ_0 is the Dirac measure of 0. Then it is well-known that $\beta=-m\ln\mathbf{r}$ with $r=|\mathbf{r}|=\sqrt{x^2+y^2}$. Through some direct calculation, the TIE becomes

$$\begin{aligned}-k\frac{\partial I}{\partial z}&=\nabla\cdot\left(I\nabla\phi_s\right)-m\nabla I\cdot\nabla\times\ln\mathbf{r}\\&=\nabla\cdot\left(I\nabla\phi_s\right)-m\left(I_x,I_y\right)\cdot\left(-\frac{y}{r^2},\frac{x}{r^2}\right)\\&=\nabla\cdot\left(I\nabla\phi_s\right)-\frac{m}{r^2}\frac{\partial I}{\partial\theta},\end{aligned} \tag{S.6}$$

where m is the topological charge of the singularity and θ is the polar angle measured about the dislocation. r can also be considered as the distance between the singularity and $\mathbf{r}$ in physics.

According to the reference [3], the multivalued phase associated with multiple phase singularities (k in total) can be added directly:

$$-k\frac{\partial I}{\partial z} = \nabla \cdot (I \nabla \phi_s) - \sum_{i=1}^{k} \frac{m_i}{{r_i}^2} \frac{\partial I}{\partial \theta_i}, \tag{S.7}$$

where m_i is the topological charge of the i_{th} vortex (singularity) and θ_i is the polar angle measured about the i_{th} vortex (dislocation).

Appendix B. The validatory simulation for the derived TIE

In the previous studies, when the wave field is coherent or in a stationary state, its spatial part may be written as $U(\mathbf{r}) = \sqrt{I(\mathbf{r})} \exp[i\varphi(\mathbf{r})/\hbar]$, where $I(\mathbf{r})$ is the probability density, $\varphi(\mathbf{r})$ is the phase, and $\hbar$ is the reduced Planck constant. The probability current is time-invariant and assumes the form $j(\mathbf{r}) = I(\mathbf{r}) \nabla\varphi(\mathbf{r})/m$, where m is the mass of the object [4]. Then the normalized probability current in terms of the ensemble-average current describes a well-defined vector field, when it is over regions of non-zero time-averaged probability density. Therefore, it can be divided into a potential and a rotational component through Helmholtz decomposition theorem [5]. The probability current can be rewritten as the following form [4]:

$$\langle j(\mathbf{r}) \rangle = \frac{1}{m} I(\mathbf{r}) [\nabla \phi_s(\mathbf{r}) + \nabla \times \beta(\mathbf{r})]. \tag{S.8}$$

This equation defines the scalar phase $\phi_s(\mathbf{r})$, which is single-valued, and the vector phase $\beta(\mathbf{r})$. This decomposition is unique up to a vectorial constant that may float between the two components and this vectorial constant is placed in the gradient term. The phase so defined obeys the Poisson-type differential equations [6]: $\nabla^2 \phi_s(\mathbf{r}) = \nabla \cdot \langle j(\mathbf{r}) \rangle$, $\nabla^2 \beta(\mathbf{r}) = -\nabla \times \langle j(\mathbf{r}) \rangle$.

Under the paraxial approximation, optical fields have been termed as [6, 7]

$$\begin{aligned} \frac{p}{\hbar}\frac{\partial I(\mathbf{r})}{\partial z} &= k\frac{\partial I(\mathbf{r})}{\partial z} = -\nabla \cdot [I(\mathbf{r}) \nabla\varphi(\mathbf{r})] \\ &= -\nabla \cdot [I(\mathbf{r}) \nabla\phi_s(\mathbf{r})] - \nabla I(\mathbf{r}) \cdot \nabla \times \beta(\mathbf{r}). \end{aligned} \tag{S.9}$$

Then considering the case of a field containing a discontinuous phase distribution, it has been established that phase dislocations may, in general, be considered as a

sum of screw and edge dislocations [8], and the multi-valued phase associated with multiple screw dislocations may be added directly [3]. It follows that Eq. S.9 may be written in the form [7, 9] (the TIE for optical vortex beams in the previous form):

$$-k\frac{\partial I(\mathbf{r})}{\partial z} = \nabla \cdot [I(\mathbf{r})\nabla\phi_s(\mathbf{r})] + \sum_i \left(\frac{m_i}{r_i}\frac{\partial}{\partial\theta_i}\right) I(\mathbf{r}), \tag{S.10}$$

where m_i is the topological charge of the i_{th} dislocation, r_i is the distance between the i_{th} dislocation and $\mathbf{r}$, and θ_i is the polar angle measured about the i_{th} dislocation. It follows, therefore, that the presence of screw dislocations has a characteristic signature in the propagation of the probability distribution. It should be noted that this expression derived by Nugent and Pangain [6, 7, 9] is similar with the new one, and the previous form has been used in several instances in the literature by Allen *et al.*[10, 11, 12]. It can be observed that there are two different parts of the equation from the previous formula, which are the sign and the denominator. The different sign may result from the definition of the rotation direction of the vortex beam. The different denominator is caused by the missing of a distance index r_i in the previous formula, which result in failing to correctly predict the intensity transport corresponding to the vortex component, and thus, the previous formula cannot be used for the quantitative phase recovery of vortex beams.

To verify the validity of the newly derived TIE (Eq. S.6), first of all, we guarantee that this formula must take effect in the divergence-free cases. In the first simulation, the uniform intensity distribution which is azimuthal symmetry around the phase singularity is shown in Fig. S.1(a1), the counterpart of which is the non-azimuthally symmetric distribution of the intensity as shown in Fig. S.1(b1). The phase distribution is a shifted astigmatism function defined on a 256×256 grid: $\varphi(\mathbf{r}) = \phi_s = 10r_x^2 - 10r_y^2 - 0.7r_x + 2r_y + 0.82$, which is single-valued and continuous, as shown in Figs. S.1(a2,b2). It should be noted that since there is no phase singularity in Figs. S.1(a2,b2), the description of "azimuthal symmetry around the phase singularity" mentioned above refers to the central point of the simulation image. This simulation indicates that the intensity distribution is azimuthal symmetry of the center point of the image. From Figs. S.1(a4,b4,a5,b5), we can find that only one kind of phase (a scalar potential function) will manifest itself, contributing to the longitudinal intensity variations, which matches with the traditional TIE.

Then we verify that Eq. S.6 can also be applied to the situation that the intensity distribution around singularity is azimuthally symmetric as shown in Figs. S.2 (a1,b1). The intensity angular derivative $[\partial I/(r^2 \cdot \partial\theta)]$ will approach zero theoretically. Figures S.2 (a4,b4) show the intensity angular derivative with the topological charge $m = \pm 1$ of the vortices, and we can find that the mean value of the whole

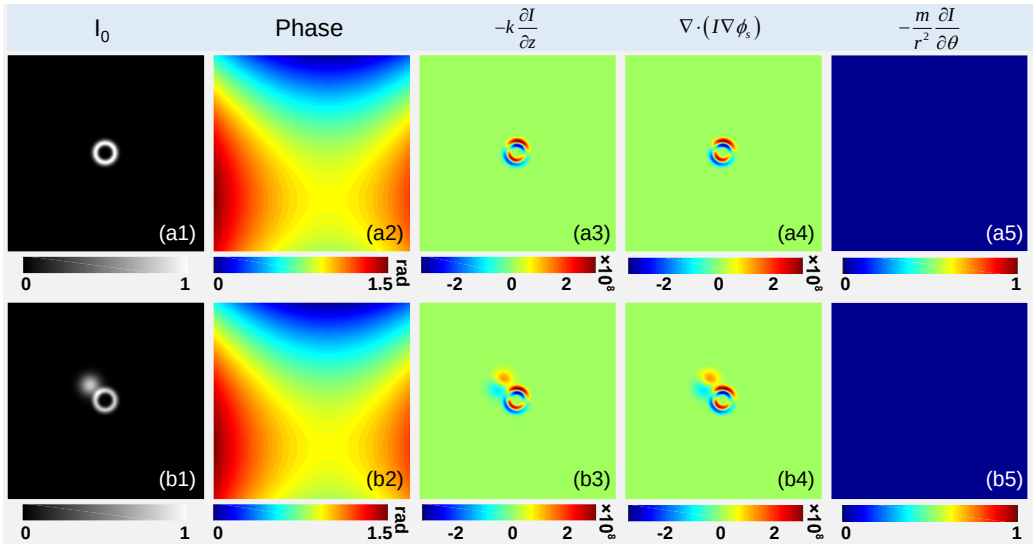

Figure S.1: The simulation with the scalar phase distribution. (a1-b1) Intensity distribution. (a2-b2) Phase distribution. (a3-b3) Longitudinal intensity derivative distribution. (a4-b4) The effect of the scalar phase. (a5-b5) Intensity angular derivative distribution.

distribution almost is zero, although the values of derivatives have minor volatility around the singularity. This discrepancy can be ignored with the values in the order of 10^{-4} due to the low sampling rate near the phase singularity. For similar reasons, we can also find that the axial derivative value of intensity is also in the order of 10^{-3}, resulting from the numerical calculation errors. Thus, in the range of allowable error, the longitudinal and angular derivative distribution of the intensity can be ignored with the given phase distribution. As a comparison, we also give the intensity angular derivative distribution of the vortex term in the previous TIE form (Eq. S.9) as shown in Figs. S.2 (a5,b5), which are also can be ignored within the allowable error range. This also indicates that the traditional TIE (*i.e.* the phase is single-valued and continuous) usually ignores this additional term.

To verify the correctness of Eq. S.6, in this case, it is necessary to ensure that there is no gradient phase which means that only the divergence-free term (screw dislocations) is included. There is no perfect method to determine whether such a phase as shown in Figs. S.2 (a2,b2,c2,d2) contains the gradient phase term, therefore on the basis of the above simulation, only the intensity distribution is changed to verify that the phase as shown in Figs. S.2 (a2,b2,c2,d2) only has the screw dislocation term, and the longitudinal and angular intensity derivative distributions are shown in Figs. S.2 (c3,c4,d3,d4). When the intensity distribution is not azimuthally symmetric around the phase singularity, we can find that the longitudinal and angu-

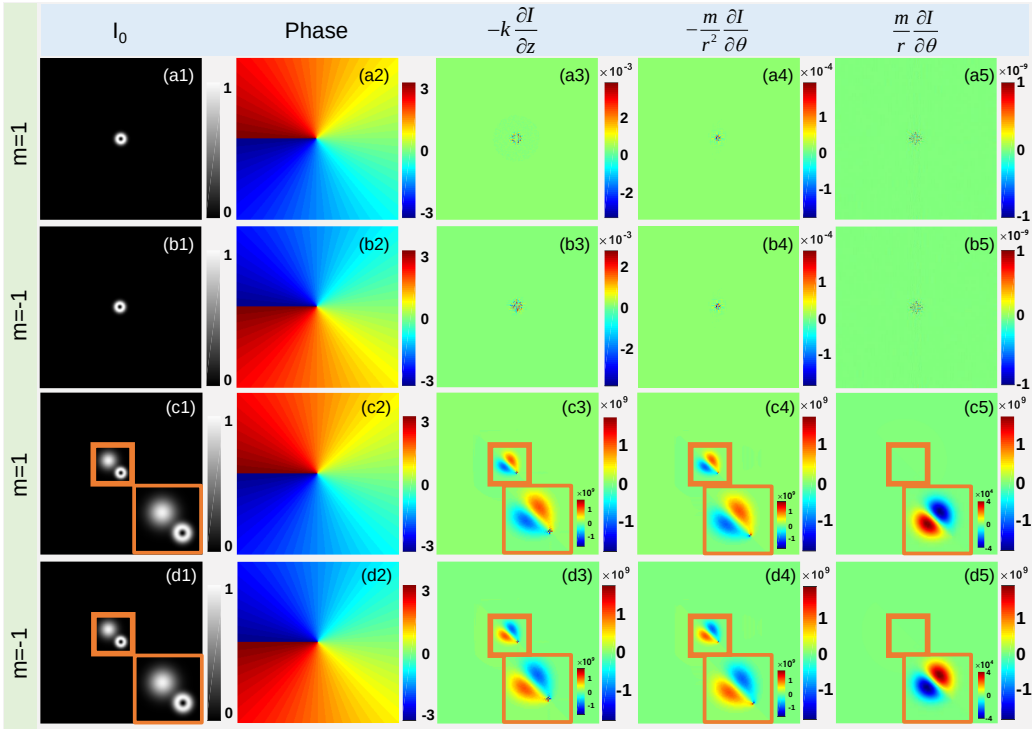

Figure S.2: The simulation with the vortex phase distribution. (a1-d1) Intensity distribution. (a2-d2) Phase distribution. (a3-d3) Longitudinal intensity derivative distribution. (a4-d4) Intensity angular derivative distribution. (a5-d5) The previous intensity angular derivative distribution.

lar intensity derivative distribution are essentially equal, which indicates that there is no effect of the gradient phase on defocusing intensity. Comparing with the results provided by the intensity angular derivative term (related to the vortex phase) in the previous TIE (Eq. S.9), as shown in Figs. S.2 (c5,d5), we can find that the numerical range of the angular intensity derivative term provided by Eq. S.9 is much lower than the longitudinal intensity derivative distribution obtained by the simulation [Figs. S.2 (c3,d3)]. From the above analysis that the gradient phase is not included in the phase distribution [Figs. S.2 (c2,d2)], so theoretically, the distribution of the longitudinal intensity derivative distribution should be determined by vortex phase. So the previous form (Eq. S.9) may not be completely accurate. In addition to verifying the correctness of the formula only with the existence of the vortex phase, from Figs. S.2 (c1-d4), we can find that in order to obtain the information related to the vortex phase field from the longitudinal intensity derivative distribution, the intensity on the focal plane must not be azimuthally symmetric around the phase singularity. Thus, it can be concluded that: *In the case of phases hidden by symmetry, the scalar*

phase may be recovered but the vector phases remain completely undetermined. Thus, to recover the hidden phases, symmetry needs to be broken. More discussion will take place below.

Finally, in order to verify the validity of the equation under more complicated situations, we add the scalar phase [the distribution is shown in Figs. S.1 (a2,b2)] to the standard vortex phase (here the topological charge of the vortices is ± 5). According to Figs. S.3 (a1-a5,b1-b5), we can see that when the intensity distribution is azimuthally symmetric around the phase singularity, the longitudinal intensity derivative distribution is almost only affected by the scalar phase, that is, the effect of the vortex phase on it is not reflected in the value (the angular intensity derivative distribution approaches a constant 0 within the allowable error range). In this case, the hidden phases are not recoverable, but, since the scalar phase is continuous, it will be uniquely recovered. Similar to before, Figs. S.3 (a6,b6) show the angular intensity derivative distribution provided by Eq. S.9, which can also be regarded as zero and ignored. Thus, in the case of phases hidden by symmetry, the scalar phase can be reconstructed, but the vortex phases remain completely undetermined. Set against that, when the intensity distribution is not circularly symmetric, the effect of the scalar phase and screw dislocation will be reflected in the axial intensity derivative, as shown in Figs. S.3 (c1-c5,d1-d5). It can also be found that the value of the intensity derivative distribution is exactly the sum of these two terms, which verifies the correctness and quantification of Eq. S.6. For comparison, the angular intensity derivative distributions provided by Eq. S.9 are shown in Figs. S.3 (c6,d6). Nevertheless, we can find that the overall distribution of the additional term [Figs. S.3 (c6,d6)] and the influence term of the gradient phase [Figs. S.3 (c4,d4)] will not be equal to the longitudinal intensity derivative term [Figs. S.3 (c3,d3)]. Therefore, Eq. S.9 is inaccurate in the quantitative expression of the influence of the vortex phase on the axial intensity derivative distribution.

Generally, the physical picture implied by Eq. S.6 is that the effect of the scalar phase is a lateral translation and the effect of the screw dislocations is a rotation as we move along z. Furthermore, the presence of the screw dislocations (vortex phase) has a characteristic signature in the propagation of the intensity distribution at the focal plane. As a result of the simulations mentioned above, we can conclude that the topological phase components may be hidden by symmetries in the intensity distribution at the focal plane. Furthermore, for the ergodic field, the measurement of the intensities over two or more measurement planes will in principle allows translation and rotation effects to be identified and decoupled [13]. The introduction of an aperture to break the azimuthal-symmetry intensity distribution can generate signals related to the screw dislocation at the boundary, so the topological charge can be

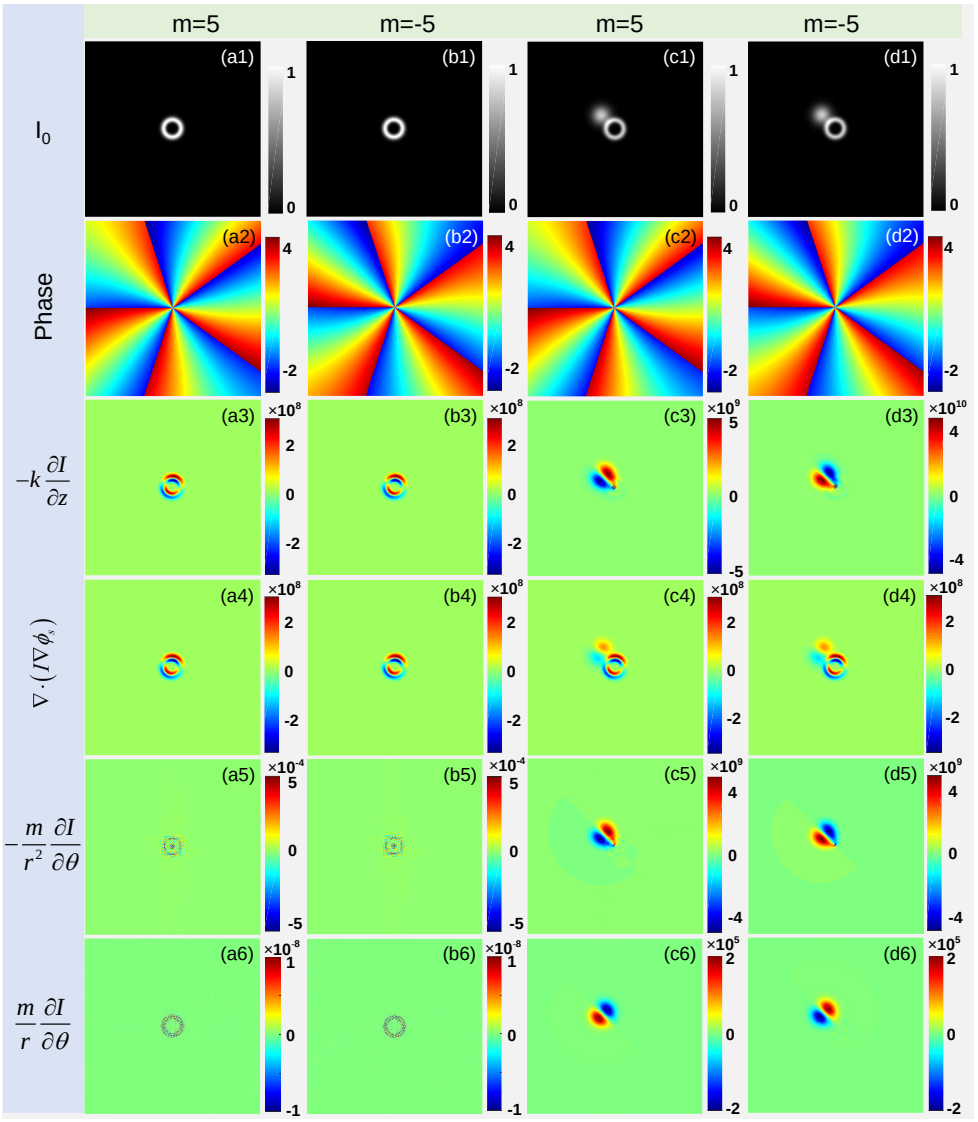

Figure S.3: The simulation with the scalar and vortex phase distribution. (a1-d1) Intensity distribution. (a2-d2) Phase distribution. (a3-d3) Longitudinal intensity derivative distribution. (a4-d4) The effect of the scalar phase. (a5-d5) Angular intensity derivative distribution. (a6-d6) The previous angular intensity derivative distribution.

distinguished.

Appendix C. Boundary conditions

Based on Eq. S.4, if the vector phase $\nabla \times \beta$ is such that ∇I and $\nabla \times \beta$ are everywhere perpendicular, this component of the phase will be invisible. In other words, the vector phase components may be hidden by symmetries in the probability density distribution. In this case, the hidden phases will be not recoverable, but since the scalar phase is continuous, it will be uniquely recovered. This is also very consistent with the conclusion of **Appendix B**: **In the case of phases hidden by symmetry, the scalar phase may be recovered but the vector phases remain completely undetermined. Thus, to recover the hidden phases, symmetry needs to be broken.**

Let us consider a particular intensity distribution in the object plane ($z = 0$): the intensity I is smooth (but can be non-uniform) in Ω but suddenly vanishes with a step-like discontinuity at the boundary $\partial\Omega$. Physically, it is equivalent to capturing intensity images through a hard-edged aperture at the object plane:

$$I = A_\Omega I_0 = \begin{cases} I_0 & \mathbf{r} \in \overline{\Omega} \\ 0 & others \end{cases}, \tag{S.11}$$

where I_0 is the intensity when there is no aperture, and A_Ω is the aperture function ($A_\Omega = 1$ when $\mathbf{r} \in \overline{\Omega}$, $A_\Omega = 0$ when $\mathbf{r} \notin \overline{\Omega}$). Since the intensity I is smooth inside Ω, it is reasonable to assume that its gradient on the boundary $\partial\Omega$ is dominated by the component in the boundary normal direction, which has the impulse value that equals the negative of the intensity boundary value and points outward from the domain:

$$\nabla I = \begin{cases} -I\delta_{\partial\Omega}\mathbf{n} & \mathbf{r} \in \partial\Omega \\ \nabla I_0 & \mathbf{r} \in \Omega \\ 0 & others \end{cases}, \tag{S.12}$$

where $\delta_{\partial\Omega}$ is the Dirac delta function around the aperture edge $\partial\Omega$ and $\mathbf{n}$ is an outward pointing unit vector, normal to $\partial\Omega$. Strictly speaking, the gradient ∇I does not exist in calculus since I is discontinuous at $\partial\Omega$. So we call ∇I here generalized gradient. Here we adopted the notation $\delta_{\partial\Omega}$ that was first used by Roddier [14] as a plausible representation of the physical quantity concentrated on the boundary curve. The $\delta_{\partial\Omega}$ can be loosely thought of as the gradient magnitude of the aperture function $\delta_{\partial\Omega} = |\nabla A_\Omega|$ or interpreted as the limit of a sequence of smooth functions. Mathematically, the function $\delta_{\partial\Omega}$ is an extension of the Dirac delta function $\delta_{\mathbf{r}}$ at a single point $\mathbf{r}$, which can be rigorously defined as a distribution such that for any

test function $f(\mathbf{r})$ that is smooth and compactly supported

$$\iint_{\mathbb{R}^2} f(\mathbf{r})\,\delta_{\partial\Omega} d\mathbf{r} = \oint_{\partial\Omega} f(\mathbf{r}) ds, \tag{S.13}$$

Substituting Eqs. S.11 and S.12 into the TIE (Eq. S.6), we can obtain:

$$\begin{aligned} -k\frac{\partial I}{\partial z} = A_\Omega \Bigg(& I_0 \nabla^2 \phi_s + \nabla I_0 \cdot \nabla \phi_s - \frac{m}{r^2}\frac{\partial I_0}{\partial \theta} \Bigg), \\ & - I\frac{\partial \phi_s}{\partial n}\delta_{\partial\Omega} + \frac{I}{r^2} m \delta_{\partial\Omega}(-y, x)\,\mathbf{n} \end{aligned} \tag{S.14}$$

The first term on the right-hand side (RHS) of Eq. S.14 is the intensity variation inside the domain due to the phase slope, curvature and rotation as if the aperture is not present. For the case of light fields with vortex phase, $\partial I_0/\partial\theta$ is usually zeros, and this term will be simplified into the form as derived in reference [15]. When there is no vortex phase $[(I/r^2)\,\delta_{\partial\Omega}\mathbf{n} = 0]$, the second term is a delta-function-like a sharply peaked signal at the aperture boundary, which is usually used for the boundary-artifact-free scalar phase retrieval [15]. When the non-circular symmetric hard apertures are introduced $[(I/r^2)\,\delta_{\partial\Omega}\mathbf{n} \neq 0]$, for this degenerate case (there are singularities resulting from the phase vortex within the region), the value of boundary condition will change according to different topological charges.

Appendix D. Uniqueness of the multi-vortex combination

Due to the addictiveness of the phase vortex, the boundary signals corresponding to different vortices are linearly independent, and can thus be directly superimposed. Then when multiple vortices exist and $(x_i, y_i), i = 1, ..., k$ are centers of the vortices, the boundary conditions will be changed into

$$\begin{aligned} -k\frac{\partial I}{\partial z} = A_\Omega \Bigg(& I_0 \nabla^2 \phi_s + \nabla I_0 \cdot \nabla \phi_s - \sum_{i=1}^{k} \frac{m_i}{{r_i}^2}\frac{\partial I_0}{\partial \theta_i} \Bigg) \\ & - I\frac{\partial \phi_s}{\partial n}\delta_{\partial\Omega} + I\delta_{\partial\Omega}\sum_{i=1}^{k} \frac{m_i\left[-(y-y_i), (x-x_i)\right]\cdot\mathbf{n}}{{r_i}^2}, \end{aligned} \tag{S.15}$$

where $r_i^2 = (x - x_i)^2 + (y - y_i)^2$, for $i = 1, 2, ..., k$. m_i is the topological charge of the i_{th} vortex (singularity) and θ_i is the polar angle corresponding to the i_{th} vortex (dislocation). Usually the introduced aperture is assumed to be the square

$\Omega = [-1/2, 1/2] \times [-1/2, 1/2]$. We will show that, for any smooth function g defined on $\partial\Omega$, the solution $(m_1, m_2, \cdots, m_k)$ of the equation is unique.

$$\sum_{i=1}^{k} \frac{m_i \left[-\left(y - y_i\right), \left(x - x_i\right)\right] \cdot \mathbf{n}}{{r_i}^2} = g \quad on \quad \partial\Omega \ . \tag{S.16}$$

This property is equivalent to the following conclusion. So we only need to prove the following lemma.

Lemma If $(m_1, m_2, \cdots, m_k)$ is a solution to the system of equations

$$\sum_{i=1}^{k} \frac{m_i \left[-\left(y - y_i\right), \left(x - x_i\right)\right] \cdot \mathbf{n}}{{r_i}^2} = 0 \quad on \quad \partial\Omega \ , \tag{S.17}$$

then $m_i = 0$, $i = 1, \cdots, k$.

Proof The assumption of this lemma is

$$0 = \sum_{i=1}^{k} \frac{m_i \left[-\left(y - y_i\right), \left(x - x_i\right)\right] \cdot \mathbf{n}}{{r_i}^2} \quad on \quad \partial\Omega \ . \tag{S.18}$$

Then on the segment $\Omega = [-1/2, 1/2] \times \{x = 1/2\}$, we have

$$0 = \sum_{i=1}^{k} \frac{m_i \left[-\left(y - y_i\right), \left(1/2 - x_i\right)\right]}{{r_i}^2} \quad \forall y \in [-1/2, 1/2] \ . \tag{S.19}$$

By integrating both sides of the above equation with respect to y on the segment $[-1/2, 1/2]$, we have

$$\begin{aligned} 0 &= \sum_{i=1}^{k} m_i \int_0^y \frac{\left(y - y_i\right)}{\left(y - y_i\right)^2 + \left(1/2 - x_i\right)^2} dy \\ &= \sum_{i=1}^{k} \frac{m_i}{2} \int_0^y \frac{d\left[\left(y - y_i\right)^2 + \left(1/2 - x_i\right)^2\right]}{\left(y - y_i\right)^2 + \left(1/2 - x_i\right)^2} \\ &= \sum_{i=1}^{k} \frac{m_i}{2} \left\{\ln\left[\left(y - y_i\right)^2 + \left(1/2 - x_i\right)^2\right] - \ln\left[{y_i}^2 + \left(1/2 - x_i\right)^2\right]\right\}. \end{aligned} \tag{S.20}$$

Then,

$$\sum_{i=1}^{k} m_i \ln\left[{y_i}^2 + \left(1/2 - x_i\right)^2\right] = \sum_{i=1}^{k} m_i ln\left[\left(y - y_i\right)^2 + \left(1/2 - x_i\right)^2\right]. \tag{S.21}$$

So

$$\prod_{i=1}^{k}\left[y_i^2+(1/2-x_i)^2\right]^{m_i}=\prod_{i=1}^{k}\left[(y-y_i)^2+(1/2-x_i)^2\right]^{m_i}. \tag{S.22}$$

Note that the left-hand side (LHS) is a constant (*i.e.*, independent of y), and the RHS is a rational function. The above equation cannot be always hold unless $m_i = 0$, $i = 1, \cdots, k$. This completes the proof. Therefore, the product of the vortex function on the corresponding boundary and the external normal vector is linearly independent, and thus the solution to the Neumann boundary problem always exists and is unique up to an arbitrary additive constant.

Appendix E. Singularity positions determination

Before the iterative reconstruction process, it is necessary to determine the position of the vortex phase singularity and the topological charge. As illustrated in Fig. S.4, we generate standard vortex phase at different locations with the topological charge m=1. Then the captured in-focus image and the all these generated vortex phase will be composited complex amplitude to propagate to defocus surface as shown in Step1. Based the defocused images after propagation, the phase correlation (Step3) between the predicted intensity derivative (Step2) and the actual ones can be calculated, and combined into one position determination matrix. In Step4, Search the position determination matrix and the correct position for each vortex is signaled out by a peak check.

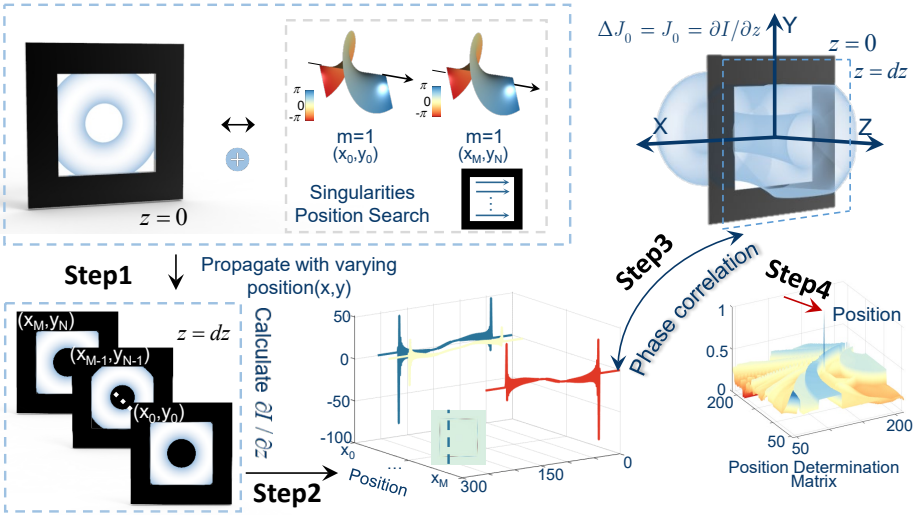

Figure S.4: The flow chart of the singularities search stage.

For the situation of the single vortex, as shown in Figs. S.5(a,e), to determine the position of the singularity, the phase correlation which estimates the relative translative offset between two similar images in the frequency domain is applied [16]. Specifically, ignoring edge effects, the discrete 2D Fourier transform is applied to both images, and the cross-power spectrum can be written as:

$$R = \frac{\mathcal{F}(g_a) \cdot \mathcal{F}^*(g_b)}{|\mathcal{F}(g_a) \cdot \mathcal{F}^*(g_b)|}, \tag{S.23}$$

where g_a is the intensity derivative distribution obtained by the captured images, and g_b is the estimated intensity derivative distribution that is generated by the captured in-focus image but with the vortex phase of the topological charge $m = 1$ and different-position singularity. In such circumstances, the phase correlation matrix $\mathcal{F}^{-1}(R)$ is a Dirac delta function theoretically. The phase correlation matrixes between the actual axial intensity derivative distribution and the predicted ones obtained at four different positions are respectively shown in Figs. S.5(b1-b4). To reduce the amount of calculation, we can only calculate all possible singularity locations in an optical field which are identified by the amplitude of the field approaching/being zero. However, considering that the peaks in each phase correlation matrix are not obvious due to a concourse of circumstances, the peak of each phase correlation matrix is then combined into a position discrimination matrix. The peak position of the position discrimination matrix will prove that this location is the singularity position, as shown in Figs. S.5(d,h). In order to distinguish the position discrimination matrix peak intuitively, we have decentralized and normalized the matrix.

In addition, considering that there may be multiple phase singularities, this phase correlation method can also be used to determine the location of these singularities, as shown in Fig. S.6. Figures S.6(a,e) give the theoretical phase distribution with the two singularities. Figures S.6(b,f) show the corresponding position discrimination matrix, and the corresponding enlargements are shown in Figs. S.6(c,g). The 3D visualization of these matrixes shown in Figs. S.6(d,h) intuitively displays the singularities position through the peak points. Here the distribution has been subtracted from the mean value and normalized. After determining the location of the singularities, according to **Appendix D**, the combination of the topological charges is unique, which can be used to compare the axial intensity derivatives generated by different combinations with the actual ones, so as to determine the final topological charges.

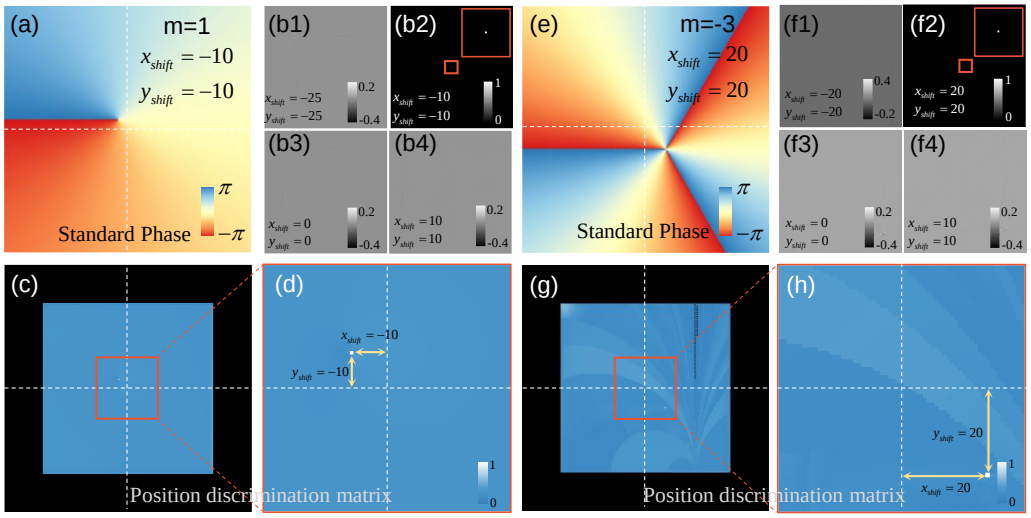

Figure S.5: Position determination of the vortex with single singularity. (a,e) The standard phase distribution with the topological charges $m = 1$ and $m = -3$. (b1-b4,f1-f4) Phase correlation distribution. (c,g) The position discrimination matrix. (d,h) The enlargement of (c,g).

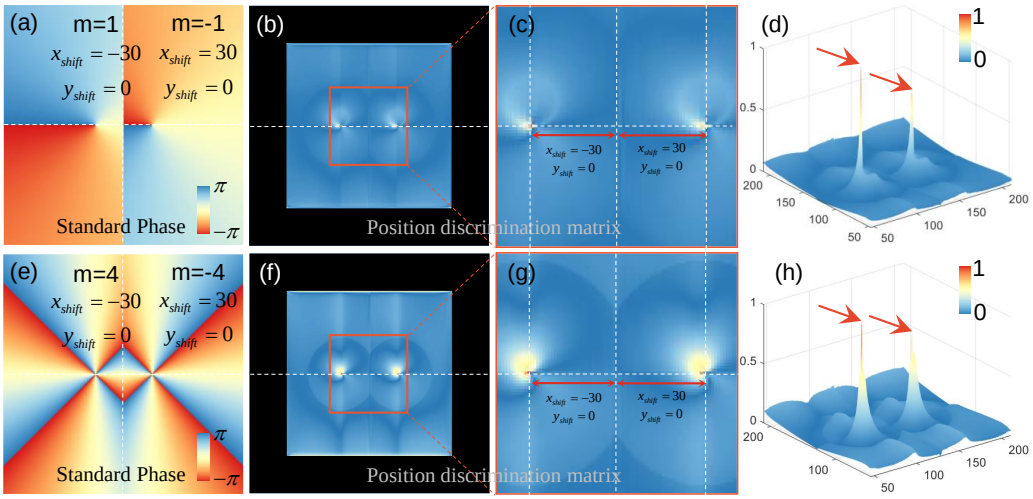

Figure S.6: Position determination of the vortex with dual singularities. (a,e) The standard phase distribution with the topological charges $m = 1\&m = -1$ and $m = 4\&m = -4$. (b,f) The position discrimination matrix. (c,g) The enlargements of the rectangular region in (b,f). (d,h) 3D visualization of (b,f).

Appendix F. Topological charges determination

After determining the location of the singularity, the search process of the topolog-

ical charge will be applied. The correct topological charge for each vortex is signaled out by a consistency check between the predicted longitudinal intensity derivative distribution (with different possible topological charge values/combinations) and the experimentally measured intensity derivative (in our example $m \in [-5, 5]$). For the single-singularity vortex, the normalized root mean square error (NRMSE) between the predicted intensity derivation and real ones is shown in Fig. S.7, the minimum point of the curve can be used to infer the topological charge value.

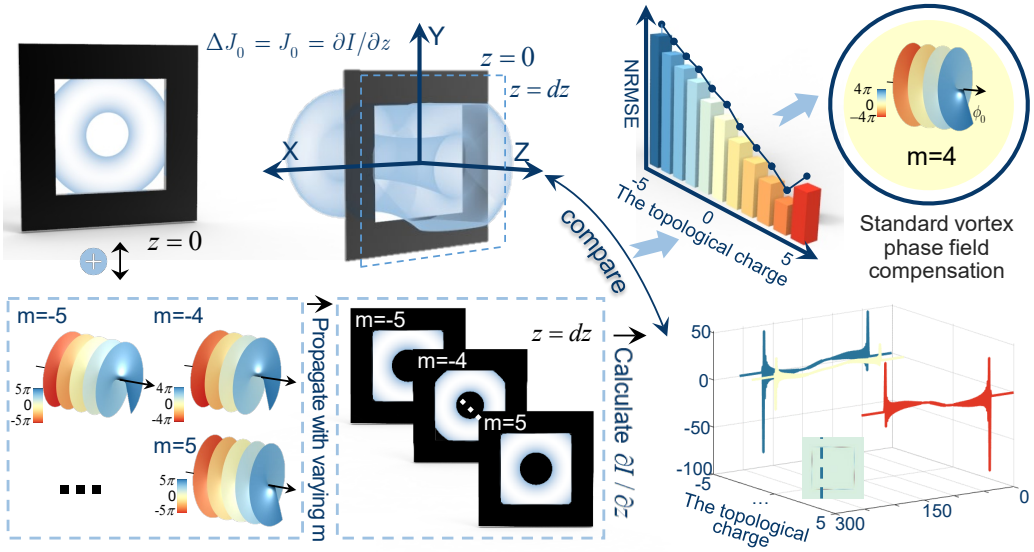

Figure S.7: The search process of the topological charge value.

Appendix G. Supplementary simulations

According to the analyses of the above-mentioned simulations, the effect of the screw dislocations (vortex phase field) can be reflected in the longitudinal intensity derivative distribution, and we will need to destroy the circular symmetry of the intensity at the focal plane as much as possible. In many cases, the intensity distribution associated with the vortex field is circularly symmetric around the phase singularity. In addition, the accuracy and validity of state-of-the-art TIE solvers need to depend on the restrictive pre-knowledge or assumptions, including appropriate boundary conditions, a well-defined closed region, and quasi-uniform in-focus intensity distribution, which, however, cannot be strictly satisfied simultaneously under practical experimental conditions [17]. Thus, we introduce a hard aperture that can not only break

the circular symmetry, but also provide the necessary boundary conditions for phase retrieval based on TIE.

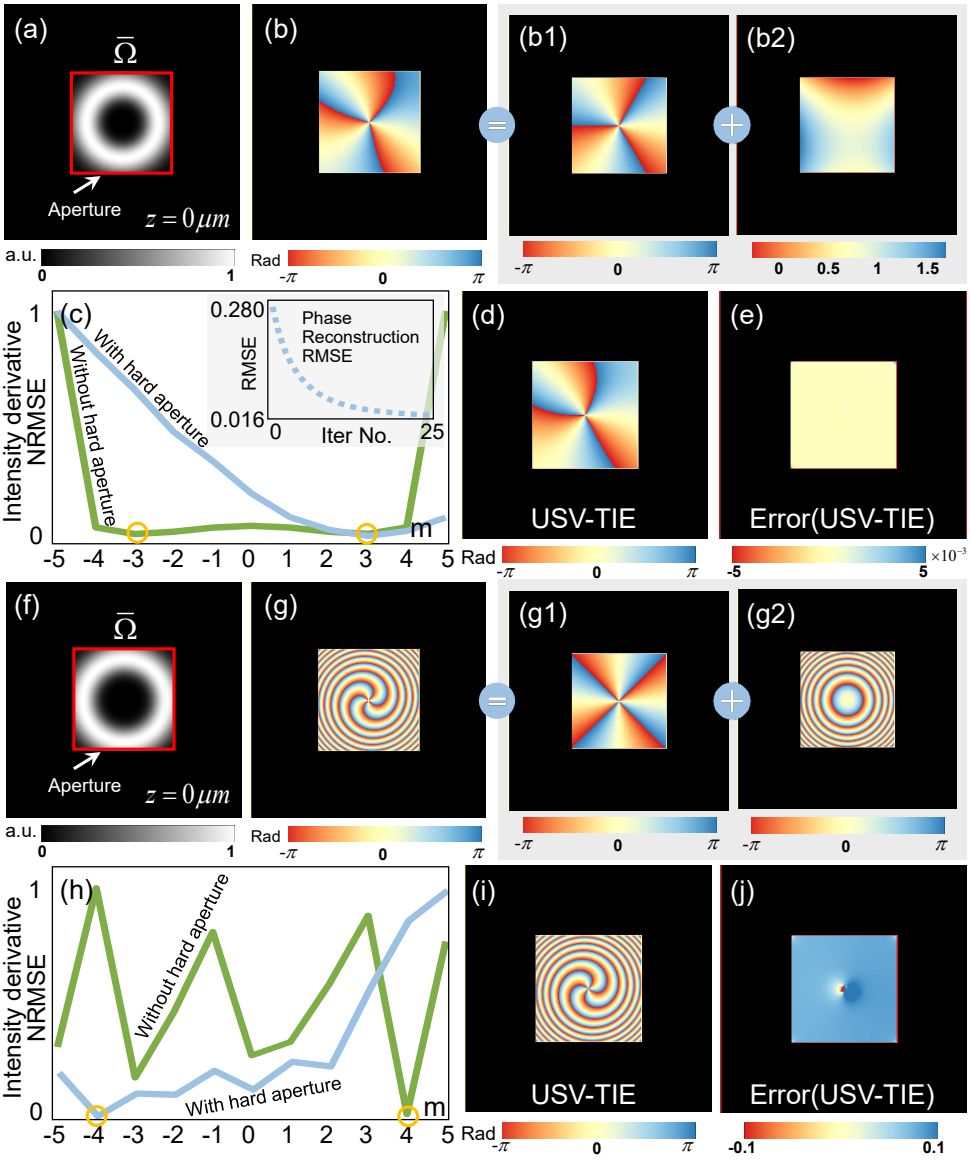

Figure S.8: The phase (scalar and vortex) retrieval based on the USV-TIE method with an aperture. (a,f) The in-focus intensity distributions with the aperture. (b,g) The simulated phase distribution with small/large scalar phase. (c,h) The NRMSE between simulated intensity derivation and real ones versus the topological charges without/with the aperture. (d,i) The reconstructed phase distribution with the USV-TIE method. (e,j) The errors corresponding to (d,i).

In order to verify the applicability of the proposed method under a wider range of conditions, the gradient phase is added to the pure vortex phase, as shown in Fig. S.8. Figures S.8(a,f) show the intensity distributions on the object plane with the aperture, which respectively corresponds to the simulated vortex phase distributions with small and large scalar phase, as shown in Figs. S.8(b,g). Figures S.8(b1,b2,g1,g2) show the standard vortex phase and additional scalar phase for simulation. Then when the above-proposed topological charge search methods are used, the NRMSE curves with the condition of the hard apertures are indicated by the blue lines in Figs. S.8(c,h), and the minimum point of which will be regarded as the final topological charge for the next step of the reconstruction process. In contrast, when there is no hard aperture, it is difficult to determine the topological charge value or even give a wrong estimation, indicated by the green lines in Figs. S.8(c,h). Here it should be emphasized here that if ϕ_s is very large (even if it submerges the distribution of vortex phase), it should be obtained by the existing iterative method called US-TIE [17] beforehand and then used for the topological charges searching. The final reconstructed results are shown in Fig. S.8(i) and the corresponding errors are shown in Fig. S.8(j). In addition, according to the comparison between the results in Fig. S.8(e) and Fig. S.8(j), when the scalar phase components at the position of the vortex phase singularity are large, the reconstructed phase error near the singularity will slightly increase, but it is still within the acceptable range. In addition, the intensity near this position is usually close to zero, and thus the phase here is not particularly significant and physically well-defined.

In addition to the single-singularity vortex phase recovery, this proposed method can also be used for phase retrieval with multiple singularities, as shown in Fig. S.9. Figures S.9(a,b) give the theoretical intensity and phase distribution, and the position discrimination matrix shown in Figs. S.9(c,d) can provide the location information of the singularities. After determining the position, the topological charge search process will be applied to explore the exact topological charge combinations, which calculates the NRMSE between the predicted axial intensity derivation and real ones for all possible combinations, as shown in Fig. S.9(e). In order to better show the specific topological charge value, the NRMSE value on the diagonal line is extracted [Fig. S.9(f)], and finally the topological charge values can be detected. The reconstructions and the corresponding errors are shown in Figs. S.9(g,h).

In addition to the above case of multiple vortices, the fractional-topological-charge vortex reconstruction can also be realized by the method mentioned in this paper. According to the above-mentioned analyses, the fractional-charge vortex can be divided into the scalar and the singular phase contribution, and thus the effect of the fractional-charge screw dislocations should also be reflected in the longitudinal in-

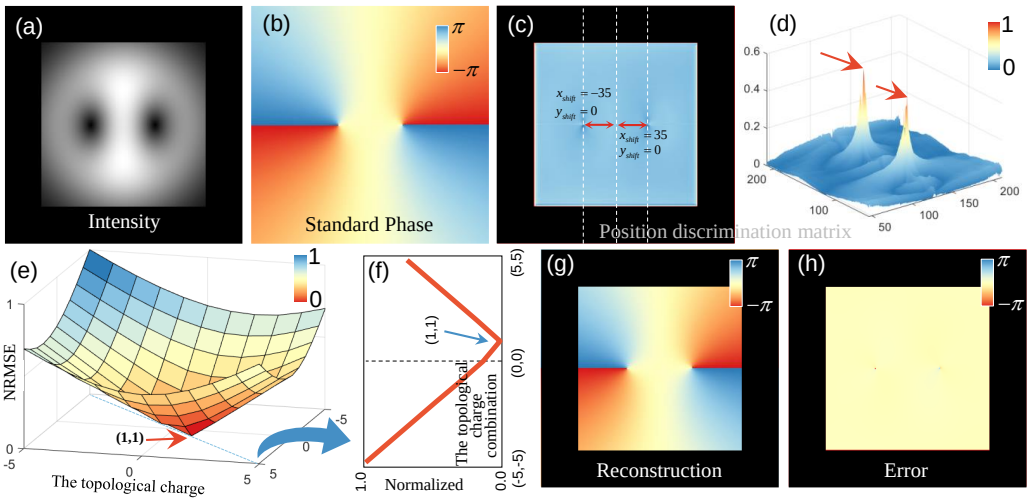

Figure S.9: The multi-singularities phase retrieval. (a,b) The theoretical intensity and phase distribution. (c) The position discrimination matrix. (d) 3D visualization of (b). (e) The NRMSE between simulated intensity derivation and real ones versus the topological charges. (f) The normalized curve of the chosen combination. (g,h) The reconstructions and corresponding error.

tensity derivative distribution. Figures S.10(a,f) give the theoretical intensity distribution, and Figs. S.10(b,g) are the phase distribution which can be divided into the corresponding two parts as shown in Figs. S.10(b1,b2,g1,g2). Then the topological charge search process is applied to explore the exact integer-topological charge, which is the number closest to the real value. During the process, the NRMSE between the predicted axial intensity derivation and real ones for all possible integer-topological charges, as shown in Figs. S.10(c,h) is calculated, and finally the singular phase contribution can be detected. Then after several rounds of iteration, the reconstructions and the corresponding errors can be obtained, as shown in Figs. S.10(d,i,e,j). In addition, according to the simulation results, it is found that the topological charge m is closer to $(2n+1)/2$ (n is an integer), the reconstruction error will be more serious. This usually results from that 1/2 included in the coefficient will introduce the phase jump of π during the scalar phase retrieval.

Appendix H. Structure diagram of the digital holographic measurement system

Figure S.11 shows the system which can not only generate hologram, but also capture the original image of TIE by moving camera. It should be noted that, the SLM is designed to work with a linearly polarized incident beam, so we add a polarizer

after the laser source. In our experiment, the rotation of the Poynting vector for a linear polarized beam arises from the effect of OAM. When the CGH pattern is loaded with a blazed grating, maximum optical power is concentrated in the $\pm 1^{st}$ diffraction orders while the residual power in the other orders is minimized, and the intensity of the $\pm 1^{st}$ diffraction orders is equal. We added an additional iris (Standard Iris) in the experiment to roughly filter higher diffraction orders ($\pm 2^{nd}$,

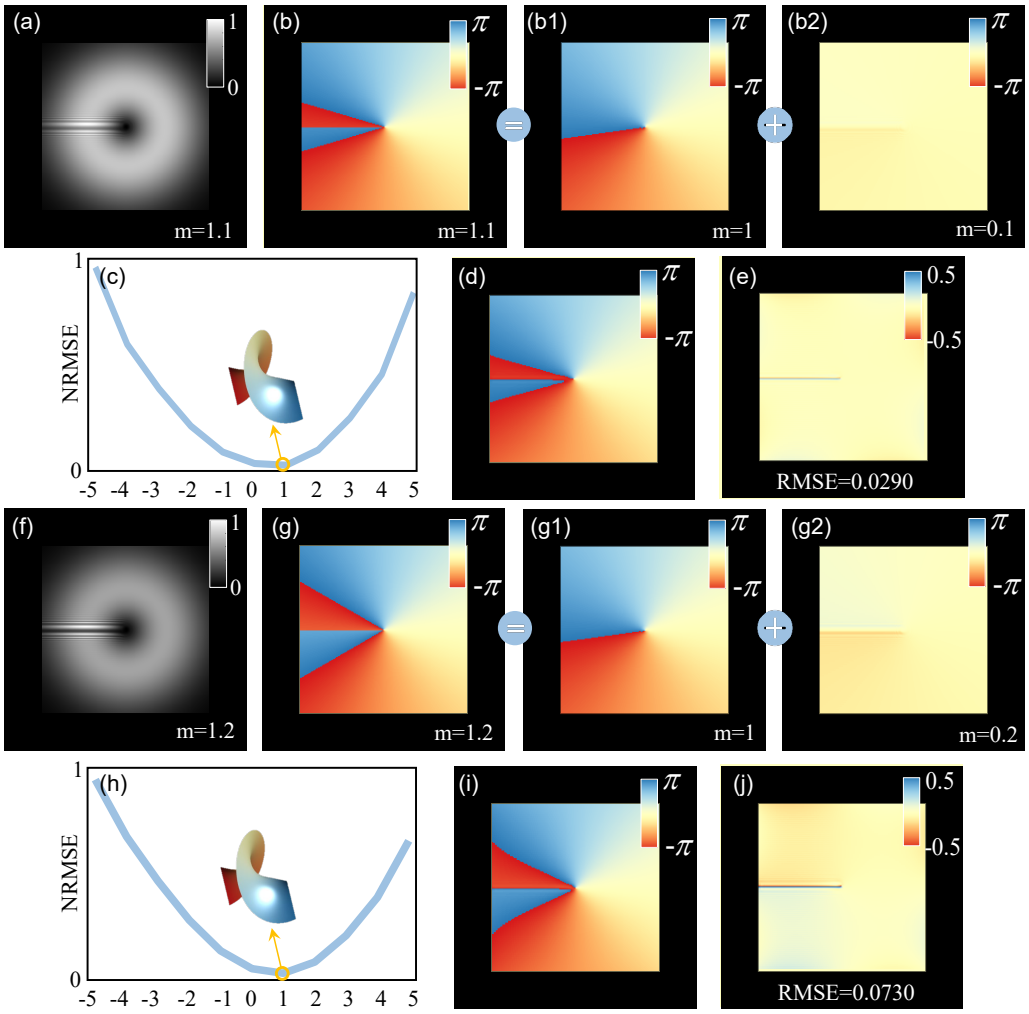

Figure S.10: The fractional-topological-charge vortex reconstruction. (a,f) The theoretical intensity distribution. (b,g) The theoretical phase distribution. (c,h) The NRMSE between simulated intensity derivation and real ones versus the topological charges with the aperture. (d,e,i,j) The reconstructions and corresponding errors.

$\pm 3^{rd}$ and higher) output from SLM. The second iris placed at the Fourier plan is to accurately select the $+1^{st}$ or -1^{st} diffraction order information. To match the pixel size of the camera, the angle between reference beam and object beam is about 3°. It may be emphasized here that since the core of the USV-TIE method is the longitudinal intensity derivative distribution, it is very important for the accuracy of intensity measurement. Thus, the cameras with large bit depth should be selected as far as possible. In this experiment, it is generally necessary to select a camera with 10bit (at least) depth.

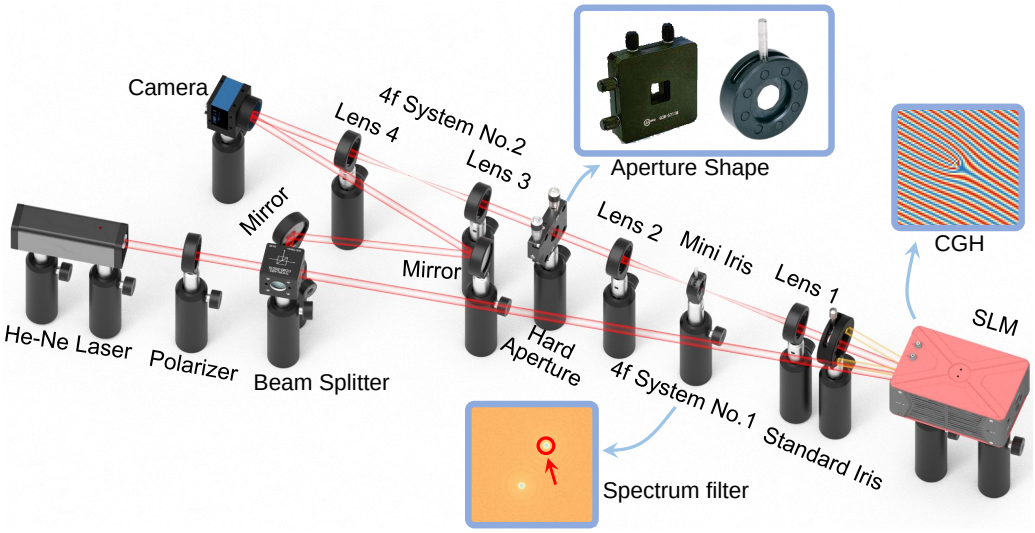

Figure S.11: The hologram and optical vortex beam generation system.

References

[1] M. R. Teague, Deterministic phase retrieval: a green's function solution, J Opt Soc Am 73 (11) (1983) 1434–1441.

[2] M. R. Dennis, K. O'Holleran, M. J. Padgett, Singular optics: optical vortices and polarization singularities, Prog Opt 53 (2009) 293–363.

[3] V. V. Voitsekhovich, D. Kouznetsov, D. K. Morozov, Density of turbulence-induced phase dislocations, Appl Opt 37 (21) (1998) 4525–4535.

[4] A. Messiah, Quantum mechanics, Vol. 1, North-Holland Publishing Company, 1961.

[5] P. M. Morse, H. Feshbach, Methods of theoretical physics, Am J Phys 22 (6) (1954) 410–413.

[6] D. Paganin, K. A. Nugent, Noninterferometric phase imaging with partially coherent light, Phys Rev Lett 80 (12) (1998) 2586.

[7] K. Nugent, D. Paganin, Matter-wave phase measurement: a noninterferometric approach, Phys Rev A 61 (6) (2000) 063614.

[8] I. Basistiy, M. Soskin, M. Vasnetsov, Optical wavefront dislocations and their properties, Opt Commun 119 (5-6) (1995) 604–612.

[9] D. Paganin, K. A. Nugent, Noninterferometric phase determination, Adv Imaging Electron Phys 118 (2001) 85–127.

[10] L. J. Allen, H. M. L. Faulkner, K. A. Nugent, M. Oxley, D. Paganin, Phase retrieval from images in the presence of first-order vortices, Phys Rev E 63 (3) (2001) 037602.

[11] L. J. Allen, H. M. L. Faulkner, M. Oxley, D. Paganin, Phase retrieval and aberration correction in the presence of vortices in high-resolution transmission electron microscopy, Ultramicroscopy 88 (2) (2001) 85–97.

[12] A. Martin, L. Allen, Phase imaging from a diffraction pattern in the presence of vortices, Opti Commun 277 (2) (2007) 288–294.

[13] J. A. Schmalz, T. E. Gureyev, D. M. Paganin, K. M. Pavlov, Phase retrieval using radiation and matter-wave fields: validity of teague's method for solution of the transport-of-intensity equation, Phys Rev A 84 (2) (2011) 023808.

[14] F. Roddier, Curvature sensing and compensation: a new concept in adaptive optics, Appl Opt 27 (7) (1988) 1223–1225.

[15] C. Zuo, Q. Chen, A. Asundi, Boundary-artifact-free phase retrieval with the transport of intensity equation: fast solution with use of discrete cosine transform, Opt Express 22 (8) (2014) 9220–9244.

[16] H. Foroosh, J. B. Zerubia, M. Berthod, Extension of phase correlation to subpixel registration, IEEE Trans Image Process 11 (3) (2002) 188–200.

[17] J. Zhang, Q. Chen, J. Sun, L. Tian, C. Zuo, On a universal solution to the transport-of-intensity equation, Opt Lett 45 (13) (2020) 3649–3652.